Geomechanics and Engineering, *Vol. 39, No. 1 (2024) 105-113*
https://doi.org/10.12989/gae.2024.39.1.105

Effect of geometry of underground structure and electrode on electrical resistance measurement: A numerical study

Tae-Young Kim[1a], Hee-Hwan Ryu[2b], Meiyan Kang[3a], Suyoung Choi[3c] and Song-Hun Chong*[1]

[1]*Department of Civil Engineering, Sunchon National University, 255 Jungang-ro, Sunchon, Jeollanam-do 57922, Republic of Korea*
[2]*Transmission & Substation Laboratory, Korea Electric Power Corporation (KEPCO) Research Institute, Daejeon 34056, Republic of Korea*
[3]*Department of Mathematics, Ajou University, 206 World cup-ro, Yeongtong-gu, Suwon-si, Gyeonggi-do, Republic of Korea*

(*Received June 11, 2024, Revised August 22, 2024, Accepted August 25, 2024*)

Abstract. Recently, electrical resistivity surveys have been used to obtain information related to underground structures including burial structure type and depth. However, various field conditions hinder understanding measured electrical resistance, and thus there is a need to understand how various geometries affect electrical resistance. This study explores the effect of geometric parameters of a structure and electrodes on electrical resistance in the framework of the finite element method. First, an electrical resistance module is developed using the generalized mesh modeling technique, and the accuracy of the module is verified by comparing the results with the analytical solution for a cylindrical electrode with conical tip. Then, 387 cases of numerical analysis including geometric parameters of a buried structure and electrodes are conducted to quantitatively estimate the detection depth under a steady-state current condition. The results show that electrical resistance is increased as (1) shallower burial depth of structure, (2) closer distance between ground electrode and structure, (3) longer horizontal electrode distance. In addition, the maximum detection depth corresponding to converged electrical resistance is deeper as (4) closer distance between ground electrode and structure, (5) shorter horizontal electrode distance. The distribution of the electric potential around the electrodes and underground structure is analyzed to provide a better understanding of the measured electrical resistance. As engineering purpose, the empirical equation is proposed to calculate maximum detection depth as first approximation.

Keywords: cylindrical electrode with conical tip; electrical resistivity survey; electrical resistance module; generalized mesh modeling technique; maximum detection depth

1. Introduction

Unexpected accidents occur during the construction of underground spaces because subsurface geophysical and geological surveys fail to detect the existence of anomalies (e.g., fault and weak zones). Therefore, advanced geophysical techniques are required to accurately predict geological conditions and prevent accidents. The method of ground-penetrating radar (GPR) has been employed in a wide range of applications, such as soil and rock profiling, water-table detection and bedrock identification, identifying structural features in underground, and bars checking in reinforcement and beam columns (Venkateswarlu and Tewari 2014, Abdelmawla *et al.* 2023). However, GPR has limitations including low resolution, shallow detection depth, antenna gain effect, and soil water content (Neal 2004). While the seismic method has been applied for a similar purpose with GPR method, blasting for the generation of signal sources has technical difficulties, such as environmental noise, installation of sensor arrays to predict the direction and location of underground structures, and the destruction of segment linings installed during tunnel excavation (Ma and Qian 2020).

The electrical resistivity method has a relatively high resolution and simple measurement process (i.e., easy installation of sensors and no additional excitation source) and thus is the most applied techniques in geophysical methods to characterize the subsurface at multiple scales, from a few centimeters to kilometers (Liu *et al*. 2008, Flechsig *et al*. 2010, Roodposhti *et al*. 2019, Yang *et al*. 2021, Chhun and Yune 2023). It measures the electrical resistance of the ground that impedes the electrical flow (electric fields and currents) induced by potential differences among embedded electrodes. Then, the measured electrical resistance is converted using a geometrical factor to quantify the intrinsic properties of the electrical resistivity. Note that the geometric factor when the field tests are preformed is a function of separation between electrodes and electrode shape, whereas these electrode properties are ignored because of their relatively small scale compared with the measuring area (Taiwo *et al*. 2017, Kim *et al*. 2023). Recently, the electrical resistivity method has been applied to different purposes of field testing. Electrical resistivity tomography (ERT) helps identify the geometries (size, shape, and location) of buried

*Corresponding author, Associate Professor
E-mail: shchong@scnu.ac.kr
[a]Graduate Student
[b]Principal Researcher
[c]Professor

ISSN: 2005-307X (Print), 2092-6219 (Online)

cavities (Cardarelli *et al*. 2006, 2010, Fasani *et al*. 2013, Olabode and San 2023) and was used to predict the characteristics of steel-tower foundations (e.g., depth, width, and span). In particular, electrical resistivity surveys has been used to obtain information related to underground structures, including the structure type and depth (Ryu *et al.* 2015, 2017). It symmetrically installs more than eight sensors along the underground structure. The resistance values from each electrode sensor were measured, and an inverse analysis was conducted. The results showed that the electrical exploration method detected more than 80% of the locations of underground structures at relatively shallow depths (less than 5 m). However, many cases related to the geometries of electrodes and underground structures provide incorrect information about the structure, and thus there is a need to understand how various geometries affect the electrical resistance,

This study explores the effect of the geometric parameters of a structure and electrodes on the electrical resistance in the framework of the finite element method. First, an electrical resistance module is developed using a generalized mesh modeling technique, and the accuracy of the module is verified by comparing the results with the analytical solution for a cylindrical electrode with conical tip. Then, extensive parametric analysis, including the geometric parameters of a buried structure and electrodes, are conducted to quantitatively estimate the detection depth under steady-state current conditions. The distribution of the electric potential around the electrodes and underground structure is analyzed to provide a better understanding of the measured electrical resistance. This discussion summarizes the variation in the maximum detection depth of a buried structure as a function of normalized distance.

2. Theoretical background: electrical resistance based on point charge

Electrical resistivity can be derived using Ohm's law and Maxwell equations. Ohm's law as empirical equation states that electric potential difference across two electrodes is directly proportional to the electric current with constant electric resistance of the medium. In addition, Gauss's flux theorem, which is a Maxwell equation, is related to the flow and distribution of the electric charge resulting from an electric field. Ohm's law can be rewritten with the current density J [amps/m^2] and electric field strength E [volts/m] when an electric field is conservative as

$$\nabla \cdot \mathrm{J} = \nabla \cdot (\sigma \cdot \mathrm{E}) = 0 \tag{1}$$

where ∇ is the Del operator and σ [1/Ω·m] is the electrical conductivity of a material. The Laplace equation, which determines the equipotential lines formed by the electric potential difference between two point-charges, can be expressed with homogeneous electrical conductivity as

$$\nabla \cdot \mathrm{J} = -\left(\underbrace{\nabla\sigma \cdot \mathrm{E}}_{=0} + \sigma \cdot \nabla \mathrm{E}\right) = \nabla^2 \mathrm{V} = 0 \tag{2}$$

After solving the second-order nonhomogeneous Euler-Cauchy differential equation, the boundary condition ($\mathrm{V} \to 0$ as the electrode distance approaches infinity) is imposed, and then the analytical formulation of the electrical potential of a single electrode can be obtained as

$$\mathrm{V} = \int \frac{\rho \cdot I}{A_{(x)}} dx \tag{3}$$

where I [amps] is the induced current flow within the medium, x [m] is the distance from the center of the electrode, and $A_{(x)}$ [m²] is the equipotential surface area as a function of the distance x from the electrode. The difference in electric potential between the appositively polarized electrodes defines the average electrical resistance as

$$\mathrm{R} = \frac{V^+ - V^-}{I} \tag{4}$$

where V^+ is positively polarized electrode, V^- is negatively polarized electrode.

In the field or a large scale, where the contact area between the electrode and medium is small and the distance between two electrodes is sufficient, the electrodes are generally assumed as a half-sphere shape with an equivalent surface area (Samouëlian *et al*. 2005). However, the electrode geometry (penetration depth, radius, and electrode distance) can change the equipotential surfaces and current flow, which eventually leads to errors of the electrical resistivity values in small-scale laboratory tests. Previous studies investigated the formulation of four electrode shapes (Hong *et al*. 2019, 2020, 2022). The electrical resistance equations for the equipotential surface and current flow are summarized in Table 1. Note that this study uses theoretical equations for cylindrical electrodes with conical tips to validate the electrical resistance numerical module.

3. Development of electrical resistance simulation module

3.1 Finite element mesh modeling

The commercial FEM software COMSOL Multiphysics® (2023) is employed to estimate the change of electrical resistance according to the geometric parameters of underground structure and electrodes. For the steady-state condition, the current flow induced by the difference in electric potential is simulated using the function of the stationary and electric currents built-in the direct current (DC) module. The finite element mesh modeling influences the accuracy and computational time. In particular, irregular mesh generation in the current flow hinders obtaining precise electrical resistance and producing smooth distribution of electrical field. The mapped and swept functions are employed to generalize mesh that efficiently helps to achieve consistent mesh modeling of the electrodes and buried structures and their surroundings.

Fig. 1 shows the generated mesh around the electrodes and the hollow circular structure in the 3D domain. As shown in Fig. 1(a), the 3D domain is modeled as 25 m wide (W) × 25 m long (D) × 15 m deep (H). The structure is extended to the side boundaries, and four electrodes are

Table 1 Schematic of equipotential and current flow line by induced potential different between electrodes. The equipotential surface area is based on the electrode shape. Electrical resistance is obtained from Eqs. (3) and (4). Note that an arbitrary length (z) is the distance from electrode surface to equipotential line

Electrode shape	Equipotential and current flow line	Equipotential surface A [m^2]	Electrical resistance R [Ω]
(a) Half-sphere (Hong *et al*. 2019)	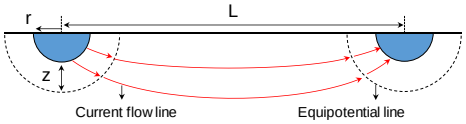	$2\pi(r+z)^2$	$\frac{\rho}{\pi}\cdot\left(\frac{1}{r}-\frac{1}{L-r}\right)$
(b) Cylinder (Hong *et al*. 2019)	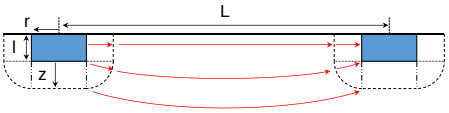	$2\pi(r+z)l+\pi^2r(1+z)+2\pi z^2$	$\frac{4\rho}{\pi(A_2-A_1)}\ln\left(\frac{4(L-2r)/A_1+1}{4(L-2r)/A_2+1}\right)$
(c) Cylindrical with half-spherical tip (Hong *et al*. 2020)	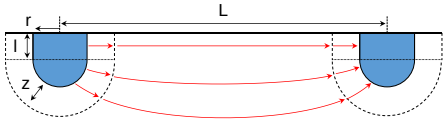	$2\pi(r+z)l+2\pi(r+z)^2$	$\frac{\rho}{\pi\cdot l}\cdot\left[\ln\left(1+\frac{l}{r}\right)-\ln\left(1+\frac{l}{L-r}\right)\right]$
(d) Cylindrical with half-conical tip (Hong *et al*. 2022)	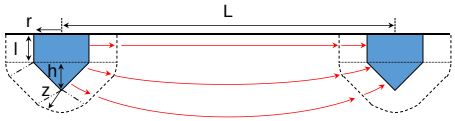	$2\pi\left(h+r\tan^{-1}(r/h)+l\right)z+\pi r\left(\sqrt{h^2+r^2}+2l\right)+2\pi z^2$	$\frac{2\rho}{\pi\cdot(B_1-B_2)}\cdot\left[\ln\left(\frac{(L-2r)/B_1+0.5}{(L-2r)/B_2+0.5}\right)\right]$

$$A_1=\pi r+2l-\sqrt{(\pi r+2l)^2-8\cdot(2rl+r^2)} \qquad B_1=h+r\cdot\tan^{-1}(r/h)+l-\sqrt{\left(h+r\cdot\tan^{-1}(r/h)+l\right)^2-2r\left(\sqrt{h^2+r^2}+2l\right)}$$

$$A_2=\pi r+2l+\sqrt{(\pi r+2l)^2-8\cdot(2rl+r^2)} \qquad B_2=h+r\cdot\tan^{-1}(r/h)+l+\sqrt{\left(h+r\cdot\tan^{-1}(r/h)+l\right)^2-2r\left(\sqrt{h^2+r^2}+2l\right)}$$

installed on the surface. Fig. 1(b) shows the width W divided into four parts (W_e, W_s, W_1, and W_2). W_e, including the electrodes, has relatively dense mesh element size of 0.05 m/element (m/elt). W_s, composing the underground structure, is modeled with mesh elements of straight lines extending in parallel with the 3D domain and has a mesh element size of approximately 0.2 m/elt. W_1 and W_2 are modeled with relatively loose mesh element sizes of approximately 0.5 m/elt. While W_1 and W_2 are changed according to the distance between the structure and electrodes, and the element size within each part remains constant. The length D is divided into three parts (W_e, D_1, and D_2). D_1 and D_2 have mesh element sizes similar to those of elements with a width W of approximately 0.5 m/elt. Fig. 1(c) shows the depth divided into four parts (W_s, H_e, H_1, and H_2). H_e, including the cylindrical part and conical tip of the electrodes, is modeled with only one mesh element for each part. H_1 and H_2 have mesh element sizes of approximately 0.2 m/elt. Furthermore, the underground structure designed extending in parallel with the 3D domain is modeled as a hollow cylinder with a thickness of 0.05 m. The electrode is modeled with a 5 mm thickness and is unfilled internally to reduce the computational time for measuring the electrical resistance of the medium between two electrodes [Fig. 1(d)]. A generalized mesh size modeled around the electrodes, and the structure is summarized in Fig. 1(e). The proposed mesh sizes are used for all numerical simulations.

3.2 Geometry and electrical resistance properties

The electrical resistivity of the electrode is assigned as AISI 303 stainless steel (Chu and Ho 1978) and the ground is assumed as sandy soil corresponding to 10% water content and 76% initial relative density (Melo *et al*. 2021). The underground structure is modeled as a polyvinyl chloride pipe (Ramesh *et al*. 2000). As an electrical boundary condition, 1 V is applied into one electrode (terminal electrode) and the other electrode is set as the ground electrode. A voltage-sweeping function is applied to the terminal electrodes to automatically obtain the electrical resistance between them. A total of 387 cases are simulated, including the distance between the two electrodes L, the burial depth of the structure d, the diameter of the structure D, and the distance between the structure and electrode u. The geometric parameters and electrical properties of the electrodes and underground structures are summarized in Table 2.

4. Results and discussion

4.1 Validation of electrical resistance module: preliminary numerical simulation

A preliminary simulation is conducted to validate the electrical resistance module developed in this study. Fig. 2 presents an evaluation of the electrical resistance equation for a cylinder electrode with a conical tip according to the electrode distance L, where an isosurface is generated around the terminal electrode under steady-state current conditions. The electrical resistance significantly increased at a shorter electrode distance (≤1 m). However, the rate of change in the electrical resistance gradually decreased, and eventually the electrical resistance approached an asymptotic value after a certain distance (>1 m). The

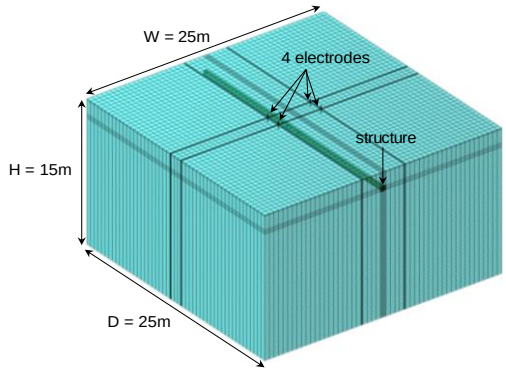

(a) 3D domain including four electrodes and structure

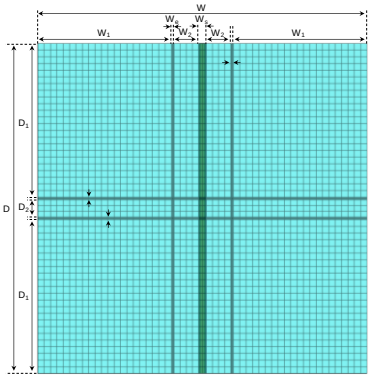

(b) Top view

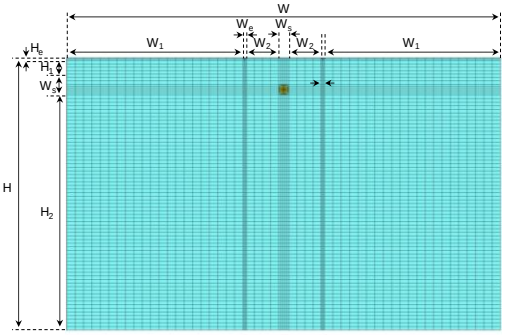

(c) Side view

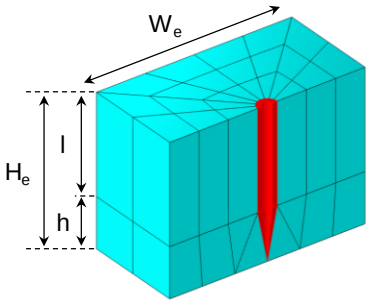

(d) Electrode geometry

Symbol	Size [m]	Symbol	Size per element [m/elt]
W_1	4.9, 10.15, 11.65	$W_{1\text{-elt}}$	≈ 0.5
W_2	$25 - 2W_1 - 2W_e - W_s$	$W_{2\text{-elt}}$	≈ 0.5
W_s	0.6	$W_{s\text{-elt}}$	≈ 0.2
W_e	0.2	$W_{e\text{-elt}}$	0.05
D_1	10.4, 11.4, 11.65, 11.9	$D_{1\text{-elt}}$	≈ 0.5
D_2	0.8, 1.3, 1.8, 3.8	$D_{2\text{-elt}}$	≈ 0.5
H_1	0.1, 0.5, 0.9, 1.3, 1.7, 2.5, 2.7, 3.2, 4.1, 4.3, 4.5, 5.3, 6.5, 7.7, 8.9, 10.3, 11.7	$H_{1\text{-elt}}$	≈ 0.2
H_2	$15 - H_e - H_1 - W_S$	$H_{2\text{-elt}}$	≈ 0.2
H_e	0.15		

(e) Generalized mesh size

Fig. 1 Generated mesh and generalized mesh size around electrode and structure proposed in this study. The proposed mesh sizes are used for all cases

Table 2 Geometry and electrical resistivity of the electrode and underground structure used in this study

Parameter				Value
Geometry [m]	Electrode	Height	Radius r	0.01
			Cylinder part l	0.1
			Conical tip part h	0.05
		Distance	Horizontal L_x	1.5, 4.5, 15
			Vertical L_y	1, 1.5, 5, 10
	Underground structure		Burial depth d	0.3, 0.7, 1.1, 1.5, 1.9, 2.7, 2.9, 3.5, 4.3, 4.5, 4.7, 5.5, 6.7, 7.9, 9.1, 10.5, 11.9
			Diameter D	0.5
			Distance from electrode u	0.45, 0.6, 0.75, 1.35, 1.8, 2.25, 4.5, 6, 7.5
Electrical resistivity [Ω·m]			Electrode ρ_e	5×10^{-7}
			Sandy Soil ρ_1	10^3
			Polyvinyl chloride pipe ρ_2	10^7

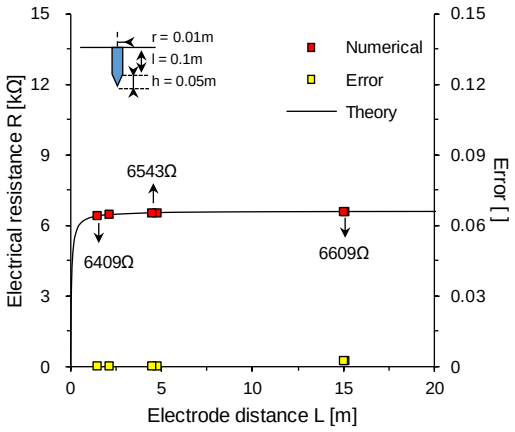

(a) Comparison between analytical solution and numerical simulation

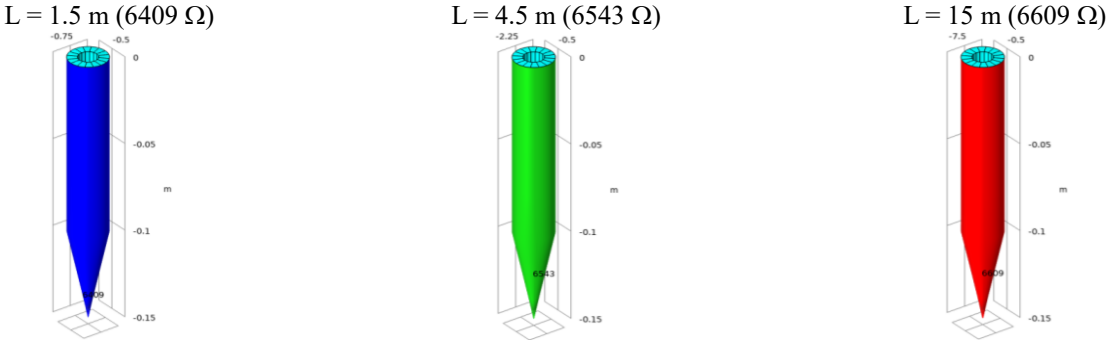

(b) Isosurface of electrical resistance around terminal electrode

Fig. 2 Verification of electrical resistance module. Continuous line indicates theoretical electrical resistance of cylindrical e lectrode with conical tip obtained from Table 1 (d)

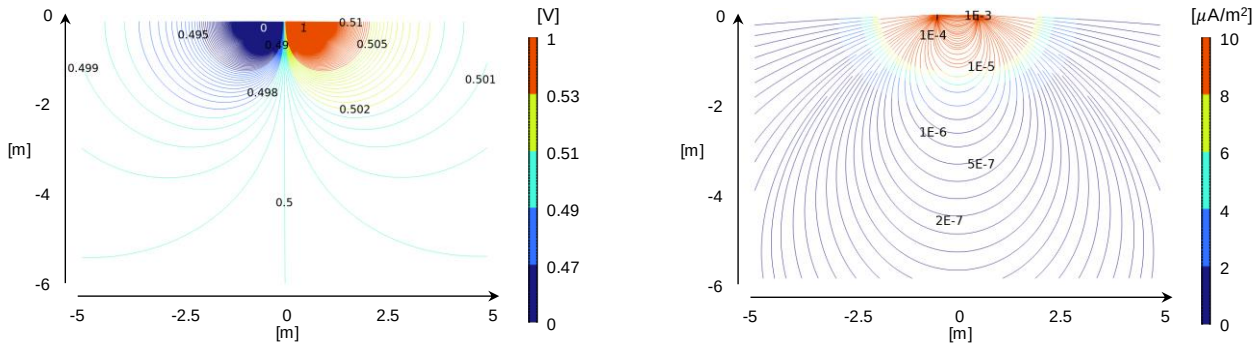

(a) Electric potential (b) Current density

Fig. 3 Distributions of (a) Electric potential and (b) Current density on the selected domain (6 m × 10 m). The current flows from the terminal electrode (right side) to the ground electrode (left side). Case is the distance between electrode L = 1.5 m and the electrical resistance R = 6409 Ω

difference between the electrical resistance values obtained from the theoretical equation and the numerical simulation are quantitatively evaluated as

$$\mathrm{ER} = \frac{|R^{Theory} - R^{Num}|}{R^{Theory}} \quad (1)$$

where R^{Theory} [Ω] is the electrical resistance value calculated using the theoretical equation, R^{Num} [Ω] is the electrical resistance value obtained from the numerical study, and ER is the error. The error is less than 0.0025 for all cases. Indeed, the proposed generalized mesh minimize the numerical error caused by mesh modeling, and the 3D domain size is sufficient to simulate the current flow and equipotential surface without boundary effects. In addition, the electrical resistance isosurface corresponding to the selected electrode distance displays a single value around the terminal electrode indicating the average electrical resistance on the electrode surface owing to the steady-state current conditions.

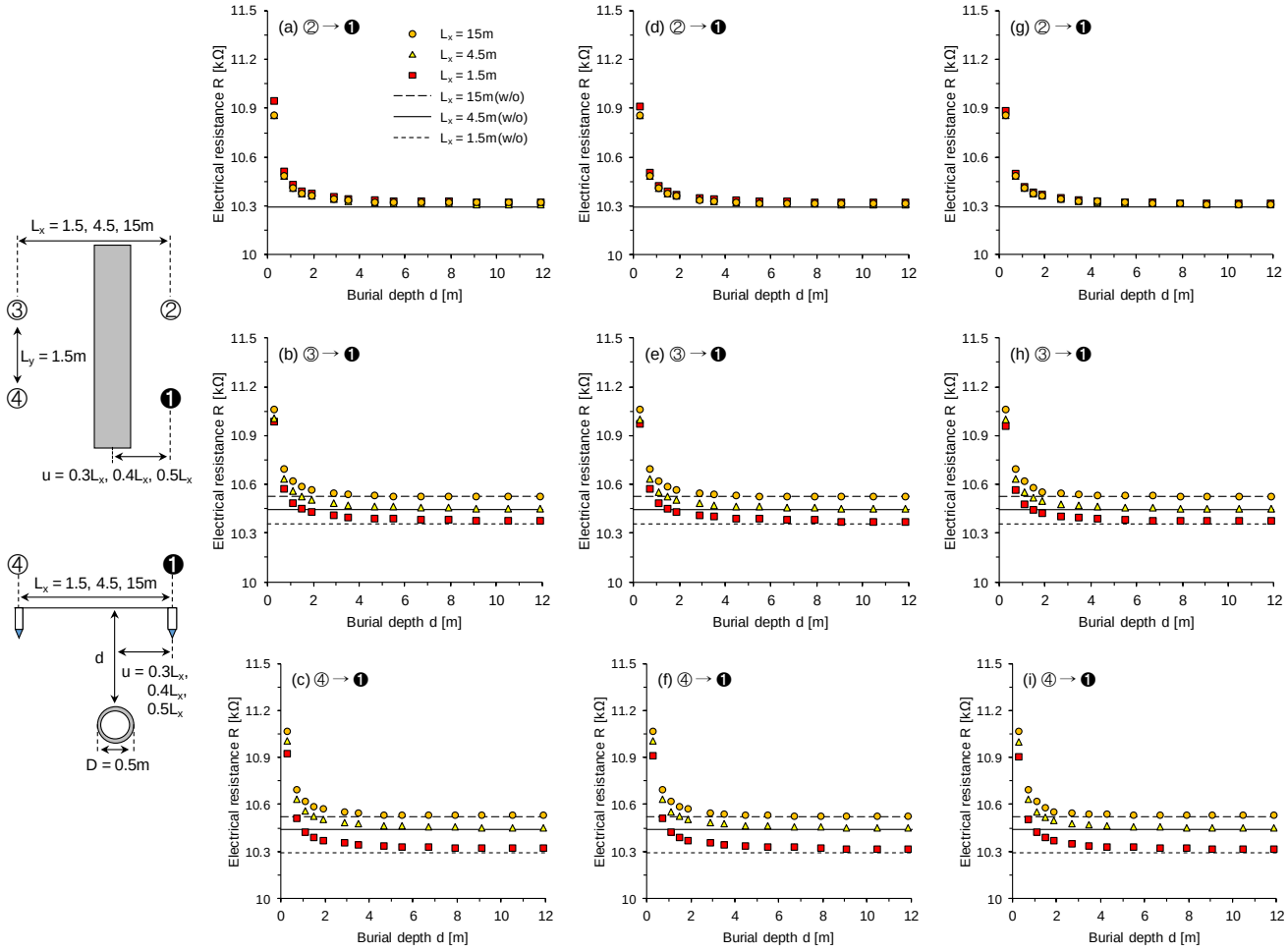

(a-c) u = 0.3L_x (d-f) u = 0.4L_x (g-i) u = 0.5L_x

Fig. 4 Variation of electrical resistance with respect to geometric parameters of underground structure and electrode. Each continuous line indicates numerical simulation results obtained in the absence of underground structure. Note that the #1 el ectrode is fixed as ground electrode, and the other electrode as terminal electrode applied 1 volt. Numerical case is L_y = 1. 5 m and D = 0.5 m

Fig. 3 shows the distribution of the electric potential and current density around the electrodes in the selected domain (6 m × 10 m). The electric potential and current density between the electrodes has symmetric distributions. The electric potential from the bottom of the terminal electrode at a depth of 0.7 m exhibits a dense distribution with a sudden voltage drop and relatively small voltage drops with loose distribution at a larger depth (>0.7 m). The current density as the amount of current flow through the cross section is proportional to the electrical field strength in the homogeneous medium ($J = \sigma \cdot E$). Indeed, the electrical resistance numerical module developed in this study is verified through a preliminary numerical simulation.

4.2 Effect of geometry parameters on electrical resistance

Fig. 4 shows the variation of electrical resistance as a function of the burial depth d with respect to three horizontal electrode distances L_x and three locations of underground structures from a close electrode under diameter D = 0.5 m and vertical electrode distance L_y = 1.5 m. Note that underground structure, which higher resistivity than the ground, hinders flowing current between electrodes. In all cases, the electrical resistance decreased with a deeper burial depth regardless the spacing between the electrodes or the structural location. In particular, a significant decrease in electrical resistance is observed up to a depth of 2 m. Subsequently, the rate of change in electrical resistance gradually decreased and eventually approached the asymptotic value obtained from the homogenous ground without an underground structure. A longer horizontal electrode distance exhibits the higher electrical resistance at the same burial depth when the terminal electrode is located from ground electrode; distance effect does not occur when both electrodes are located on the same side. In addition, the maximum detection depth corresponding to the converged electrical resistance is deeper as the horizontal distance between two electrodes become closer: a shorter electrode distance (L_x = 1.5 m) shows a deeper maximum burial depth (d = 11.9 m), whereas a longer distance (L_x = 15 m) presents a shallower maximum burial depth (d = 2.9 m) [Figs. 4(a)-4(c)]. As the

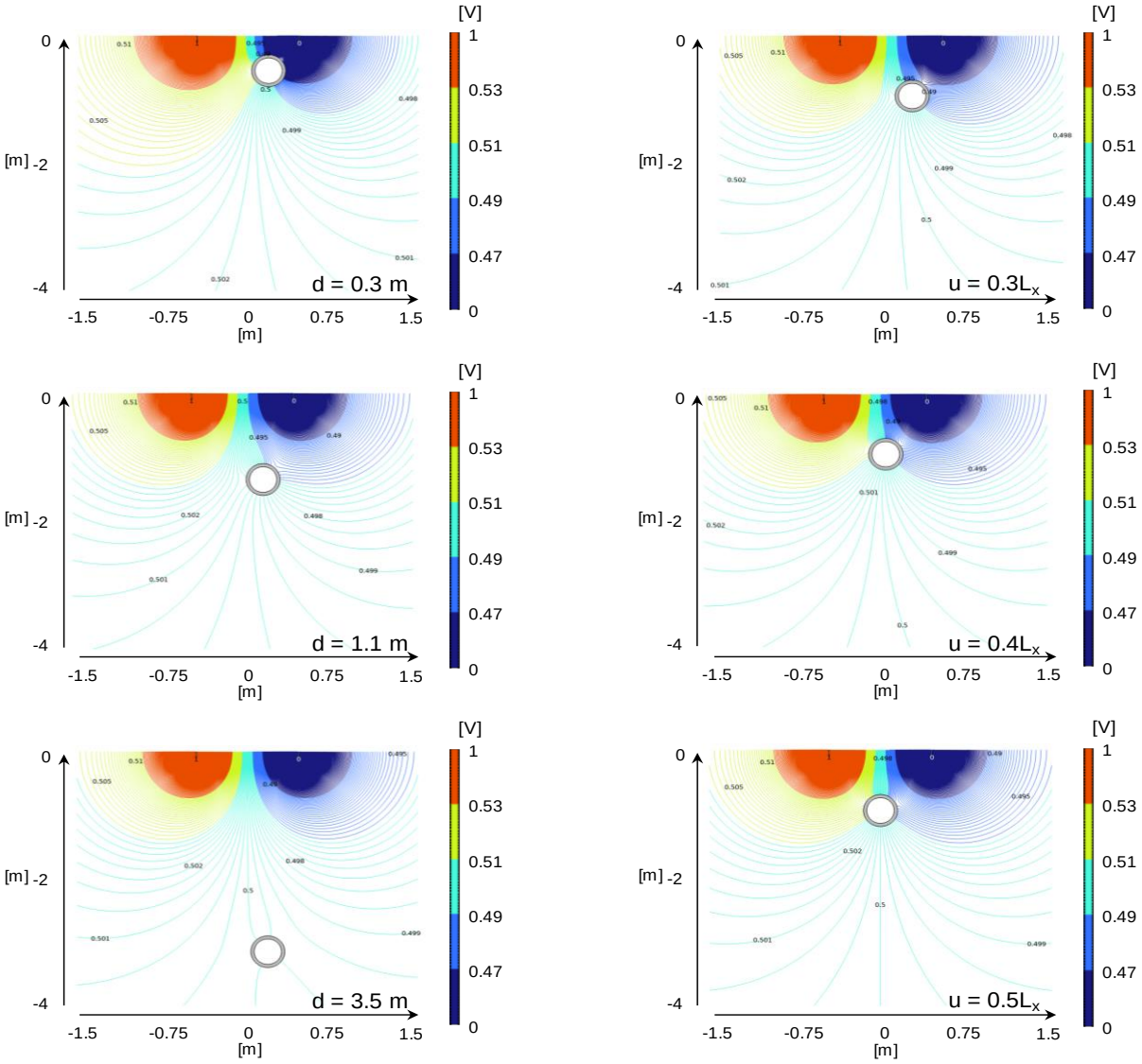

(a) Burial depth (L_x = 1.5 m) (b) Distance between structure and ground electrode (d = 0.5 m)

Fig. 5 Effect of underground structure burial depth on the voltage drop and current flow

underground structure is located far away from the ground electrode, the electrical resistance decreased and the maximum burial depth is observed at relatively shallow depth. For example, when the electrical voltage is induced at terminal electrode #4, the maximum burial depth for distance between the structure and ground electrode ($u = 0.5L_x$) is approximately 7.9 m for the L_x = 1.5 m and 2.7 m for the L_x = 15 m [Fig. 4(i)]. The detection depth is summarized on the next section. This observation underscores the importance of selecting the distance between electrodes to accurately detect underground structures at even greater depths.

Fig. 5 shows the distribution of the electric potential around two electrodes and the underground structure to understand the measured electrical resistance in the selected domain (4 m × 3 m). Clearly, the electric potential is suddenly changed around the underground structure regardless the burial depth. The structure at a shallow depth (d = 0.3 m) significantly disrupts the current flow between the electrodes, resulting in a rapid voltage drop of 0.49–0.5 V in the direction of the current flow above the structure. The buried structure at a greater depth (d = 3.5 m) exhibits a relatively gradual voltage drop (0.5 V) above the underground structure [Fig. 5(a)]. In addition, the underground structure ($u = 0.3L_x$) located relatively close to the ground electrode shows dramatically decrease in electric potential from 0.49 V to 0.495 V in above the structure. As expected, as the distance between the structure and ground electrode increased, the voltage drops of 0.5 V, and a gentle voltage drop occurred around the structure.

4.3 Discussion: detection depth

In the electrical resistivity survey, the distance between installed electrodes has critical effect on the detection depth of burial structure. This study proposes empirical equations that help to calculate the maximum detection depth d_c as a first approximation. Fig. 6 shows the maximum detection depth as a function of the normalized distance defined by the electrode position and distance between the electrodes.

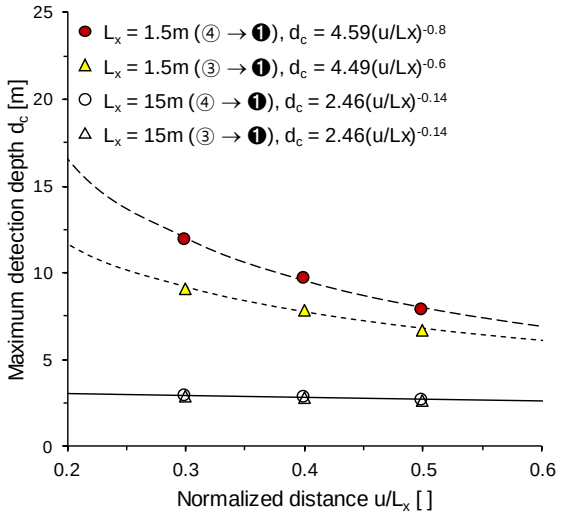

Fig. 6 Maximum detection depth as a function of normalized distance. Case is electrode distance L_y = 1.5 m and diameter D = 0.5 m. R^2 as the coefficient of determination is 0.99 in all cases

While higher electrical voltage difference increases the maximum detection depth, this study keeps the voltage difference constant. The maximum detection depth is significantly decreased as longer the distance between underground structure and ground electrode. At the same normalized distance, the maximum detection depth is greater when the terminal electrode is located close to the ground electrode; terminal electrode #4 shows a deeper maximum detection depth. Meanwhile, a sufficient horizontal distance (L_x = 15 m) exhibits a constant maximum detection depth regardless the distance between the structure and ground electrode.

5. Conclusions

This study is explored to understand the change of electrical resistance according to various geometries of structure and electrode. The 3D numerical simulations module in framework of finite-element method are developed using generalized mesh modeling technique. Total 384 cases including the geometric parameters of the underground structure and electrodes are simulated to quantitatively investigate the change in the electrical resistance. Salient conclusions are as follows:

• The mesh is modeled by using the mapped and swept functions to efficiently achieve consistent mesh of the domain. The generalized mesh modeling technique causes less error (< 0.0025) between electrical resistance values obtained from the theoretical equation and numerical simulation, implying that developed electrical resistance module is verified.

• Extensive parametric analysis shows that electrical resistance is increased as (a) longer horizontal electrode distance, (b) the shallower depth of the structure, and (c) proximity to ground electrode with structure.

• The presence of structure with high electrical resistivity than the ground disrupts the current flow between electrodes, resulting in either rapid voltage drops from ground electrode in the direction of current flow around the underground structure. Those distributions are more pronounced for shallower burial depth and shorter distance from structure to ground electrode.

• The maximum detection depth corresponding to converged electrical resistance is deeper as (d) closer horizontal electrode distance and (e) shorter the distance between structure and electrode. The empirical equation shows the relation between detection depth and normalized distance can be used to select distance between electrodes to accurately detect underground structure at even deeper depth as first approximation.

Acknowledgments

This research work was funded by Korea Electric Power Corporation, grant number R21SA02.

References

Abdelmawla, A., Ma, S., Yang, J.J. and Kim, S.S. (2023), "Subsurface anomaly detection utilizing synthetic GPR images and deep learning model", *Geomech. Eng.*, **33**(2), 203-209. https://doi.org/10.12989/gae.2023.33.2.203

Cardarelli, E., Di Filippo, G. and Tuccinardi, E. (2006), "Electrical resistivity tomography to detect buried cavities in Rome: a case study", *Near Surface Geophys.*, **4**(6), 387-392. https://doi.org/10.3997/1873-0604.2006012.

Cardarelli, E., Cercato, M., Cerreto, A. and Di Filippo, G. (2010), "Electrical resistivity and seismic refraction tomography to detect buried cavities", *Geophys. Prospect.*, **58**(4), 685-695. https://doi.org/10.1111/j.1365-2478.2009.00854.x.

Chhun, K.T. and Yune, C.Y. (2023), "Evaluation of strength characteristics of cement-stabilized soil using the electrical resistivity measurement", *Geomech. Eng.*, **33**(3), 261-269. https://doi.org/10.12989/gae.2023.33.3.261.

COMSOL Inc. (2023), http://www.comsol.com

Fasani, G.B., Bozzano, F., Cardarelli, E. and Cercato, M. (2013), "Underground cavity investigation within the city of Rome (Italy): A multi-disciplinary approach combining geological and geophysical data", *Eng. Geol.*, **152**(1), 109-121. https://doi.org/10.1016/j.enggeo.2012.10.006

Flechsig, C., Fabig, T., Rücker, C. and Schütze, C. (2010), "Geoelectrical investigations in the Cheb Basin/W-Bohemia: an approach to evaluate the near-surface conductivity structure", *Studia Geophysica et Geodaetica*, **54**, 443-463. https://doi.org/10.1007/s11200-010-0026-6.

Chu, T.K. and Ho, C.Y. (1978), "Thermal conductivity and electrical resistivity of eight selected AISI stainless steels", *Therm. Conductivity* **15**, 79-104. https://doi.org/10.1007/978-1-4615-9083-5_12.

Hong, C.H., Chong, S.H., Hong, E.S., Cho, G.C. and Kwon, T.H. (2019), "Theoretical and experimental studies on influence of electrode variations in electrical resistivity survey for tunnel ahead prediction", *J. Korean Tunn. Undergr. Sp. Assoc.*, **21**(2), 267-278. .https://doi.org/10.9711/KTAJ.2019.21.2.267

Hong, C.H., Chong, S.H. and Cho, G.C. (2020), "Electrical resistivity measurement with spherical-tipped cylindrical electrode embedded on two layers", *Materials*, **13**(9), 2144. https://doi.org/10.3390/ma13092144.

Hong, C.H., Kim, J.S. and Chong, S.H. (2022), "Theoretical

resistance in cylindrical electrodes with conical tip", *Geomech. Eng.*, **30**(4), 337-343. https://doi.org/10.12989/gae.2022.30.4.337.

Kim, T.Y., Lee, S.H., Ryu, H.H. and Chong, S.H. (2023), "Influence of electrode geometry on electrical resistivity survey: Numerical study", *J. Korean Tunn. Undergr. Sp. Assoc.*, **25**(2), 101-120. https://doi.org/10.9711/KTAJ.2023.25.2.101.

Liu, S.Y., Du, Y.J., Han, L. and Gu, M. (2008), "Experimental study on the electrical resistivity of soil–cement admixtures", *Environ. Geol.*, **54**, 1227-1233. https://doi.org/10.1007/s00254-007-0905-5

Ma, Z. and Qian, R. (2020), "Overview of seismic methods for urban underground space", *Interpretation*, **8**(4), SU19-SU30. https://doi.org/10.1190/INT-2020-0044.1.

Melo, L.B.B.d., Silva, B.M., Peixoto, D.S., Chiarini, T.P.A., Oliveira, G.C.d. and Curi, N. (2021), "Effect of compaction on the relationship between electrical resistivity and soil water content in Oxisol", *Soil Tillage Res.*, **208**, 104876. https://doi.org/10.1016/j.still.2020.104876.

Neal, A. (2004), "Ground-penetrating radar and its use in sedimentology: principles, problems and progress", *Earth-Sic. Rev.*, **66**(3-4), 261-330. https://doi.org/10.1016/j.earscirev.2004.01.004.

Olabode, O.P. and San, L.H. (2023), "Analysis of soil electrical resistivity and hydraulic conductivity relationship for characterisation of lithology inducing slope instability in residual soil", *Int. J. Geo-Eng.*, **14**(1), 7. https://doi.org/10.1186/s40703-023-00184-z

Ramesh, S. and Arof, A.K. (2000), "Electrical conductivity studies of polyvinyl chloride-based electrolytes with double salt system", *Solid State Ionics*, **136**, 1197-1200. https://doi.org/10.1016/S0167-2738(00)00598-1.

Roodposhti, H.R., Hafizi, M.K., Kermani, M.R.S. and Nik, M.R.G. (2019), "Electrical resistivity method for water content and compaction evaluation, a laboratory test on construction material", *J. Appl. Geophys*., **168**, 49-58. https://doi.org/10.1016/j.jappgeo.2019.05.015

Ryu, H.H., Cho, S.A., Kim, K.Y. and Cho, G.C. (2017), "Exploration of underground utilities using method predicting an anomaly(II) – field application", *J. Korean Tunn. Undergr. Sp. Assoc.*, **19**(3), 449-461. https://doi.org/10.9711/KTAJ.2017.19.3.449

Ryu, H.H., Kim, K.Y., Lee, K.R., Lee, D.S. and Cho, G.C. (2015), "Exploration of underground utilities using method predicting an anomaly", *J. Korean Tunn. Undergr. Sp. Assoc.*, **17**(3), 205-214. https://doi.org/10.9711/KTAJ.2015.17.3.205

Samouëlian, A., Cousin, I., Tabbagh, A., Bruand, A. and Richard, G. (2005), "Electrical resistivity survey in soil science: a review", *Soil Tillage Res.*, **83**(2), 173-193. https://doi.org/10.1016/j.still.2004.10.004

Taiwo, S.M., Lee, J.S. and Yoon, H.K. (2017), "Analytical and experimental studies to obtain electrical resistivity in a small-scaled laboratory test", *Geophysics*, **82**(5), 267-275. https://doi.org/10.1190/geo2016-0491.1

Venkateswarlu, B. and Tewari, V.C. (2014), "Geotechnical Applications of Ground Penetrating Radar (GPR)", *J.. Ind. Geol. Cong*, **6**(1), 35-46.

Yang, B., Egbert, G.D., Zhang, H., Meqbel, N. and Hu, X. (2021), "Electrical resistivity imaging of continental United States from three-dimensional inversion of EarthScope USArray magnetotelluric data", *Earth Planet. Sci. Lett.*, **576**, 117244. https://doi.org/10.1016/j.epsl.2021.117244.